May 24th - May 29th

Sand Plasticity Model for Nonlinear Seismic Deformation Analyses

Ross W. Boulanger
University of California, Davis, CA

Fifth International Conference on
Recent Advances in Geotechnical Earthquake Engineering and Soil Dynamics
and Symposium in Honor of Professor I.M. Idriss
May 24-29, 2010 • San Diego, California

SAND PLASTICITY MODEL FOR NONLINEAR SEISMIC DEFORMATION ANALYSES

Ross W. Boulanger
University of California
Davis, California, USA 95616

ABSTRACT

A sand plasticity model for nonlinear seismic deformation analyses is presented. The model follows the basic framework of the stress-ratio controlled, critical state compatible, bounding surface plasticity model for sand presented by Dafalias and Manzari (2004). Modifications to the model were implemented to improve its ability to approximate the stress-strain responses important to geotechnical earthquake engineering applications; in essence, the model was calibrated at the equation level to provide for better approximation of the trends observed across a common set of experimentally- and case history-based design correlations. An overview of the model formulation and example simulations of element loading tests are presented.

INTRODUCTION

A sand plasticity model for nonlinear seismic deformation analyses is introduced. The model follows the basic framework of the stress-ratio controlled, critical state compatible, bounding surface plasticity model for sand initially presented by Manzari and Dafalias (1997) and later extended by Dafalias and Manzari (2004). The present model incorporates several modifications designed to improve its ability to approximate the stress-strain responses important to geotechnical earthquake engineering applications. This paper provides an overview of the model formulation and example simulations of element loading tests. Details of the constitutive relationships and more extensive illustrations of the model behavior are provided in Boulanger (2010).

The continued development of nonlinear seismic deformation analysis tools is a particularly appropriate topic for this symposium in honor of Professor I. M. Idriss because, among his many contributions to our profession, he pioneered the development and application of some of our most common geotechnical earthquake engineering analysis tools and methodologies. He has followed the continued development of constitutive models and numerical platforms with great interest, and we have frequently discussed the need and roles for such tools in practice. Those discussions and his encouragement were, in fact, one of the motivating factors for my efforts on developing the model presented herein. This is just one example of the many ways in which Ed's mentorship and friendship have influenced my career over the past almost two decades.

CONSTITUTIVE MODEL OBJECTIVES

The development of the present model was guided by the need in geotechnical earthquake engineering practice for a model that can be more quickly calibrated to the engineering design relationships that are used to estimate the stress-strain behaviors that are important to predicting liquefaction-induced ground deformations during earthquakes. It is unlikely that any one model can be developed or calibrated to simultaneously fit a full set of applicable design correlations for monotonic and cyclic, drained and undrained behaviors of sand, in part because the various design correlations are not necessarily physically consistent with each other; e.g., they may include a mix of laboratory test-based and case history-based relationships, or they have been empirically derived from laboratory data sets for different sands. Nonetheless, it is desirable that a model, after calibration to the design relationship that is of primary importance to a specific project, be able to produce behaviors that are reasonably consistent with the general magnitudes and trends in other applicable design correlations or typical experimental data.

The stress-strain behaviors of a constitutive model for sand that are commonly the focus in practice include the following items.

- The cyclic resistance ratio (CRR) against triggering of liquefaction, which is commonly estimated based on SPT and CPT penetration resistances with case-history-based liquefaction correlations. The CRR is the cyclic stress ratio (e.g., CSR = τ_{cyc}/σ'_{vc}, with τ_{cyc} = horizontal cyclic shear stress, σ'_{vc}=vertical consolidation stress) that is required to trigger liquefaction in a specified number of equivalent uniform loading cycles.
- The response under the irregular cyclic loading histories produced by earthquakes, which is approximately represented by the relationship between CRR and number of equivalent uniform loading cycles. This aspect of behavior also directly relates to the magnitude scaling factors (MSF) that are used with liquefaction correlations in practice.
- The dependence of CRR on effective confining stresses and sustained static shear stresses. These aspects of behavior are represented by the K_σ and K_α correction factors, respectively, that are used with liquefaction correlations in practice.
- The accumulation of shear strains after triggering of liquefaction. Evaluations of reasonable behavior are often based on comparisons to laboratory tests results for similar soils in the literature.
- The strength loss as a consequence of liquefaction, which may involve explicitly modeling phenomena such as void redistribution or empirically accounting for it through case history-based residual strength correlations.
- The small-strain shear modulus which can be obtained through in-situ shear wave velocity measurements.
- The shear modulus reduction and equivalent damping ratio relationships prior to triggering of liquefaction. These aspects of behavior are commonly estimated using empirical correlations derived from laboratory test results for similar soils in the literature.
- The drained and undrained monotonic shear strengths, which may be estimated using correlations to SPT and CPT penetration resistances.
- The volumetric strains during drained cyclic loading or due to reconsolidation following triggering of liquefaction, both of which may be estimated using empirical correlations derived from laboratory test results for similar soils in the literature.

The utility of a nonlinear soil model in practice is dependent on: (1) its ability to approximate the above behaviors over a broad range of conditions and, (2) on the level of engineering effort required for calibrating the model. For example, a single geotechnical structure can have strata or zones of sand ranging from very loose to dense under a wide range of confining stresses and loading conditions (e.g., above and below the water table, at various points beneath a slope or foundation load, and at various levels of shaking), such that the engineering effort is greatly reduced if the constitutive model can reasonably approximate the predicted stress-strain behaviors under all these different conditions. If the model cannot approximate the trends across all these conditions, then extra engineering effort is required in deciding what behaviors should be prioritized in the calibration process, and sometimes by the need to repeat the calibrations for the effects of different initial stress conditions within the same geotechnical structure.

The information available for calibration of constitutive models in design practice most commonly includes basic soil classification tests (e.g., grain size distributions), penetration resistances (e.g., SPT or CPT), and shear wave velocity (V_s) measurements. If shear wave velocity data are not available, the V_s are often estimated based on correlations to penetration test data. More detailed laboratory tests, such as triaxial or direct simple shear tests, are almost never available due to the problems with overcoming sample disturbance effects in clean sands and the challenge of identifying representative samples from highly heterogeneous deposits.

The constitutive model described herein was developed for earthquake engineering applications, with specific goals being: (1) the ability to reasonably approximate the empirical correlations commonly used in U.S. practice, and (2) the ability to calibrate the model with a reasonable amount of effort. In essence, the approach taken was to calibrate the constitutive model at the equation level, such that the functional forms for the various constitutive relationships were chosen for their ability to approximate the important trends embodied in the extensive empirical correlations commonly used in practice.

This paper provides an overview of the model formulation and input parameters, followed by example simulations of element loading tests. Details of the model formulation and a more complete set of simulation examples are provided in Boulanger (2010).

MODEL FORMULATION

The present model follows the basic framework of the stress-ratio controlled, critical state compatible, bounding-surface plasticity model for sand presented by Dafalias and Manzari (2004). The Dafalias and Manzari (2004) model extended the previous work by Manzari and Dafalias (1997) by adding a fabric-dilatancy related tensor quantity to account for the effect of fabric changes during loading. The fabric-dilatancy related tensor was used to macroscopically model the effect that microscopically-observed changes in sand fabric during plastic dilation have on the contractive response upon reversal of loading direction. Dafalias and Manzari (2004) provide a detailed description of their model framework, beginning with a triaxial formulation that simplifies its presentation and followed by the general multi-axial formulation. The complete details of the model proposed herein is presented in

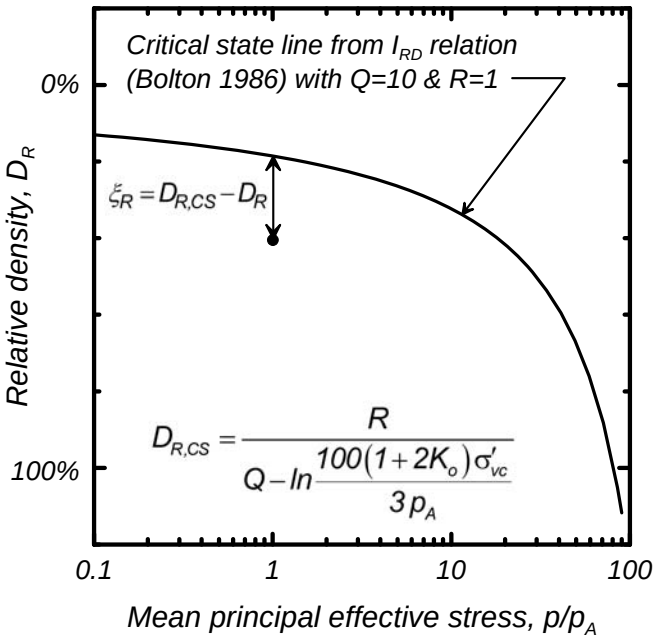

Fig. 1. Definition of the relative state parameter index, ξ_R (Boulanger 2003) and the effects of varying Q and R

its multi-axial formulation, along with the original Dafalias-Manzari model for comparison, in Boulanger (2010).

For defining critical state, the present model uses the relative state parameter index (ξ_R) as presented in Boulanger (2003) and shown in Fig. 1. The relative state parameter (Konrad 1988) is the state parameter (Been and Jefferies 1985) normalized by the difference between the maximum void ratio (e_{max}) and minimum void ratio (e_{min}) values that are used to define relative density (D_R). The relative state parameter "index" is just the relative state parameter defined using an empirical relationship for the critical state line. Boulanger (2003) used Bolton's (1986) dilatancy relationship to define the empirical critical state line and thus arrived at,

$$\xi_R = D_{R,cs} - D_R \tag{1}$$

$$D_{R,cs} = \frac{R}{Q - ln\left(100\frac{p}{p_A}\right)} \tag{2}$$

where $D_{R,cs}$ = relative density at critical state, p = the mean effective normal stress (the conventional prime symbol is dropped from the effective stress terms for convenience because all stresses are effective for the model), and p_A = atmospheric pressure (e.g., 101.3 kPa). The parameters Q and R were shown by Bolton (1986) to be about 10 and 1.0, respectively, for quartzitic sands.

The model incorporates bounding, dilation, and critical surfaces following the form of Dafalias and Manzari (2004). The present model simplifies the surfaces by removing the Lode angle dependency (e.g., friction angles are the same for compression or extension loading) that was included in the Dafalias-Manzari model, such that the bounding (M^b) and dilation (M^d) ratios can be related to the critical stress (M) ratio by the following simpler expressions.

$$M^b = M \cdot exp\left(-n^b \xi_R\right) \tag{3}$$

$$M^d = M \cdot exp\left(n^d \xi_R\right) \tag{4}$$

where n^b and n^d are parameters determining the values of M^b and M^d, respectively.

The present implementation was further simplified by casting the various equations and relationships in terms of the in-plane stresses only. This limits the present implementation to plane-strain applications and is not correct for general cases, but it has the advantage of simplifying the implementation and improving computational speed by reducing the number of operations. Expanding the implementation to include the general case should not, however, affect the general features of the model. For the present implementation, the mean normal stress p is therefore taken as the average of the in-plane normal stresses, q is the difference in the major and minor principal in-plane stresses, and the relationship for M is reduced to

$$M = 2 \cdot sin\left(\phi_{cv}\right) \tag{5}$$

where ϕ_{cv} is the constant volume or critical state effective friction angle. The three surfaces can, for the simplifying assumptions described above, be convenient visualized as linear lines on a q-p plot (where $q = \sigma_1 - \sigma_3$) as shown in Fig. 2 or as circular surfaces on a stress-ratio graph of r_{yy} versus r_{xy} as shown in Fig. 3, where r_{yy} and r_{xy} are terms from the deviatoric stress ratio tensor **r** (tensors in bold). Note that **r** = **s**/p, where **s** = the deviatoric stress tensor, $\boldsymbol{\sigma}$ = the stress tensor, $\mathbf{s} = \boldsymbol{\sigma} - p\mathbf{I}$, and **I** = the identity tensor. The stress-ratio defined yield surface is cone shaped with its size controlled by the constant m, as shown in Fig. 2. The yield surface and image back-stress ratio tensor ($\boldsymbol{\alpha}$), as shown in Fig. 3, follow those of the Dafalias-Manzari model, although their final form is considerably simplified by neglecting any Lode angle dependency.

As the model is sheared toward critical state ($\xi_R = 0$), the values of M^b and M^d will both approach the value of M. Thus the bounding and dilation surfaces move together during shearing until they coincide with the critical state surface when the soil has reached critical state.

The elastic shear modulus in the model proposed herein is dependent on the mean effective stress according to,

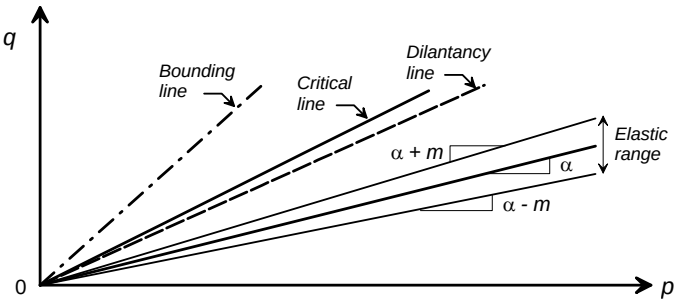

Fig. 2. Schematic of yield, critical, dilatancy, and bounding lines in q-p space (after Dafalias & Manzari 2004)

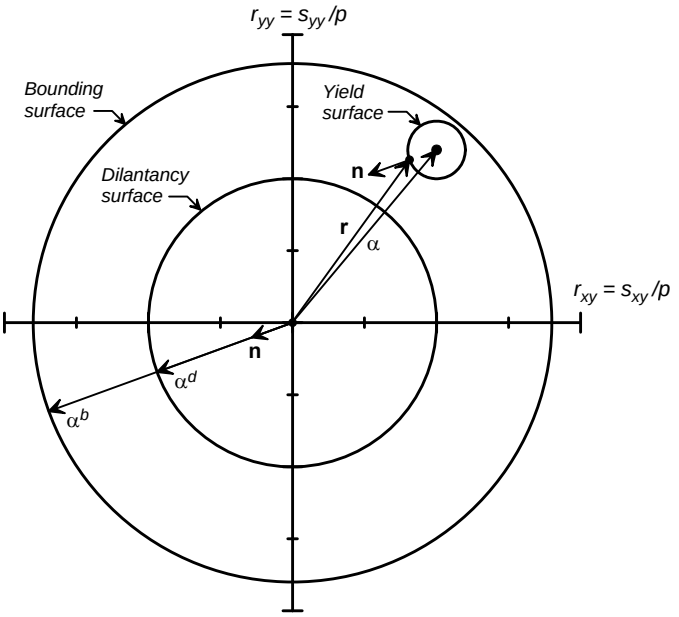

Fig. 3. Schematic of the bounding, dilation, and yield surfaces on the r_{yy}-r_{xy} stress-ratio plane with the yield surface, normal tensor, dilatancy back stress ratio, and bounding back stress ratio.

$$G = G_o p_A \left(\frac{p}{p_A}\right)^{1/2} \tag{6}$$

where G_o is a constant and p_A is atmospheric pressure. The bulk modulus is related to the shear modulus through a specified value of Poisson's ratio.

Dafalias and Manzari (2004) introduced a fabric-dilatancy tensor (**z**) that evolved in response to plastic volumetric dilation strains and could be used to account for the effects of prior straining. The fabric-dilatancy tensor was modified for the present model as,

$$d\mathbf{z} = -\frac{c_z}{1+\left\langle \frac{z_{cum}}{2z_{max}} - 1 \right\rangle} \frac{\left\langle -d\varepsilon_v^p \right\rangle}{D} \left(z_{max}\mathbf{n} + \mathbf{z}\right) \tag{7}$$

In this expression, the tensor **z** evolves in response to plastic deviatoric strains that occur during dilation only, which is represented by the MacCauley brackets ⟨⟩ which return the argument if it is positive and return zero if the argument is negative; i.e., ⟨x⟩=x if x>0, and ⟨x⟩=0 if x≤0. In addition, the rate of evolution for **z** decreases with increasing values of the cumulative value of plastic deviator strains (z_{cum}, a scalar quantity), which enables the undrained cyclic stress-strain response to progressively accumulate shear strains rather than lock-up into a repeating stress-strain loop. In addition, the greatest past peak amplitude (z_{peak}, a scalar quantity) for **z** during its loading history is also tracked. The terms c_z and z_{max} are input parameters.

The plastic modulus (K_p) in the present model is a function of the fabric history as,

$$K_p = G \cdot h_o \cdot \frac{\left[\left(\boldsymbol{\alpha}^b - \boldsymbol{\alpha}\right):\mathbf{n}\right]^{0.5}}{\left[exp\left(\boldsymbol{\alpha} - \boldsymbol{\alpha}_{in}\right):\mathbf{n} - 1\right] + C_{\gamma 1}} \cdot \frac{C_{K\alpha}}{1 + C_{Kp}\left(\frac{z_{peak}}{z_{max}}\right)\left\langle\left(\boldsymbol{\alpha}^b - \boldsymbol{\alpha}\right):\mathbf{n}\right\rangle} \tag{8}$$

where h_o is an input parameter, $C_{\gamma 1} = h_o/200$, C_{Kp} was set equal to 2.0, and $C_{K\alpha}$ is a function of the degree of stress ratio rotation. The colon means that the trace is taken of the product of the two adjacent tensors. The functional forms for the above equation were chosen because they were able to mimic empirically observed slopes for the relationship between CRR and number of equivalent uniform loading cycles in undrained loading, the empirically observed modulus reduction and damping behavior in drained loading, and the empirically observed effects of sustained static shear stress ratios.

The dilatancy relationships were also modified from those proposed by Dafalias and Manzari (2004). Different forms for expansion versus contraction, and a more complex dependence on fabric, were found to be useful. The volume change behavior during dilation (D < 0) is expressed as,

$$D = A_d \cdot \left[\left(\boldsymbol{\alpha}^d - \boldsymbol{\alpha}\right):\mathbf{n}\right] \tag{9}$$

$$A_d = \frac{A_{do}\left(C_{zin2}\right)}{\left(\frac{z_{cum}^2}{z_{max}}\right)\left(1 - \frac{\left\langle -\mathbf{z}:\mathbf{n}\right\rangle}{\sqrt{2}\cdot z_{peak}}\right)^3 \left(C_\varepsilon\right)\left(C_{pzp}\right)\left(C_{pmin}\right)\left(C_{zin1}\right) + 1} \tag{10}$$

where C_ε is an input parameter, and the terms C_{pzp}, C_{pmin}, C_{zin1}, and C_{zin2} are functions of the fabric and stress history, as

described in Boulanger (2010). Of particular interest are the first two terms in the denominator. The first term [z_{cum}^2/z_{max}] facilitates the progressive growth of strains under symmetric loading by reducing the dilatancy that occurs when a liquefied soil has been sheared through many cycles of loading; note that this term progressively increases with subsequent cycles of loading. The second term facilitates strain-hardening when the plastic shear strain reaches the prior peak value, wherein the term approaches zero (i.e., when $\mathbf{z}:\mathbf{n}$ approaches $z_{peak}\sqrt{2}$) and the dilation rate consequently rapidly approaches the virgin loading value defined by A_{do} (an input parameter).

The volume change behavior during contraction ($D > 0$) is expressed as,

$$D = A_{dc} \cdot \left[\left(\boldsymbol{\alpha} - \boldsymbol{\alpha}^{in} \right) : \mathbf{n} + C_{in} \right]^2 \frac{\left(\boldsymbol{\alpha}^{d} - \boldsymbol{\alpha} \right) : \mathbf{n}}{\left(\boldsymbol{\alpha}^{d} - \boldsymbol{\alpha} \right) : \mathbf{n} + C_D} \tag{11}$$

$$A_{dc} = \frac{A_{do}}{h_p} \tag{12}$$

where h_p is the product of an input parameter h_{po} and an internal function of ξ_R and fabric history terms, C_{in} is a function that depends on stress history, and C_D is a constant set equal to 0.10. The internal function of ξ_R was chosen to produce a reasonable effect of overburden stress on CRR. Setting D proportional to the square of $((\boldsymbol{\alpha}-\boldsymbol{\alpha}_{in}):\mathbf{n} + C_{in})$ was found to be important for obtaining a reasonable slope of the relationship between CRR and number of uniform loading cycles.

Other modifications to the constitutive relationships included: providing a constraint on the dilatancy during volumetric expansion so that it is consistent with Bolton's (1986) dilatancy relationship; adding sedimentation effects for improved estimation of reconsolidation strains following liquefaction; and modifying the logic for tracking previous initial back-stress ratios (i.e., loading history effect). A summary of the constitutive equations along with those in the Dafalias and Manzari (2004) model are provided in Boulanger (2010).

INPUT PARAMETERS

There are three primary parameters that are most important for model calibration, and a secondary set of 17 parameters that may be modified from their default values in special circumstances. The three primary input parameters are the sand's relative density D_R, the shear modulus coefficient G_o, and the contraction rate parameter h_{po}.

Relative density can be estimated in practice by correlation to penetration resistances. For example, a common form for SPT correlations is,

$$D_R = \sqrt{\frac{(N_1)_{60}}{C_d}} \tag{13}$$

where D_R is expressed as a ratio rather than a percentage. Idriss and Boulanger (2008) reviewed published data and past relationships (e.g., Cubrinovski and Ishihara 1999), and then adopted a value of $C_d = 46$ in the development of their liquefaction triggering correlations. For the CPT, they similarly reviewed available relationships (e.g., Salgado et al. 1997) and arrived at the following expression,

$$D_R = 0.465 \left(\frac{q_{c1N}}{C_{dq}} \right)^{0.264} - 1.063 \tag{14}$$

for which they adopted C_{dq}=0.9.

The second primary input parameter is the constant G_o which controls the elastic shear modulus. The elastic shear modulus can be calibrated to fit in-situ V_s measurements, according to,

$$G = \rho \cdot (V_s)^2 \tag{15}$$

or alternatively fit to values of V_s that may be estimated by correlation to penetration resistances (e.g., Andrus and Stokoe 2000).

The third primary input parameter is the constant h_{po} which is used to modify the contractiveness and hence enable calibration of the model to specific values of cyclic resistance ratio (CRR).

Secondary input parameters are those parameters for which default values have been developed that will generally produce reasonable agreement with the trends in typical design correlations. The user must, however, still confirm through element loading calibrations that the default parameters are appropriate for their particular conditions. The secondary input parameters are described in Boulanger (2010), along with commentary on the recommended default values.

EXAMPLE RESPONSES

The model was implemented as a user defined material for use with the commercial program FLAC (Itasca 2009). The response of the model is illustrated in Boulanger (2010) for initial relative densities of 35%, 55%, and 75% with corresponding SPT $(N_1)_{60}$ values of approximately 6, 14, and 26, respectively. Values for G_o were obtained using a form of the correlation by Andrus and Stokoe (2000). Values for h_{po} were obtained by calibrating the model to obtain the $CRR_{M=7.5}$ values computed using the SPT-based liquefaction triggering correlation by Idriss and Boulanger (2008). All secondary input parameters were assigned their default values. Simulations were presented for drained and undrained,

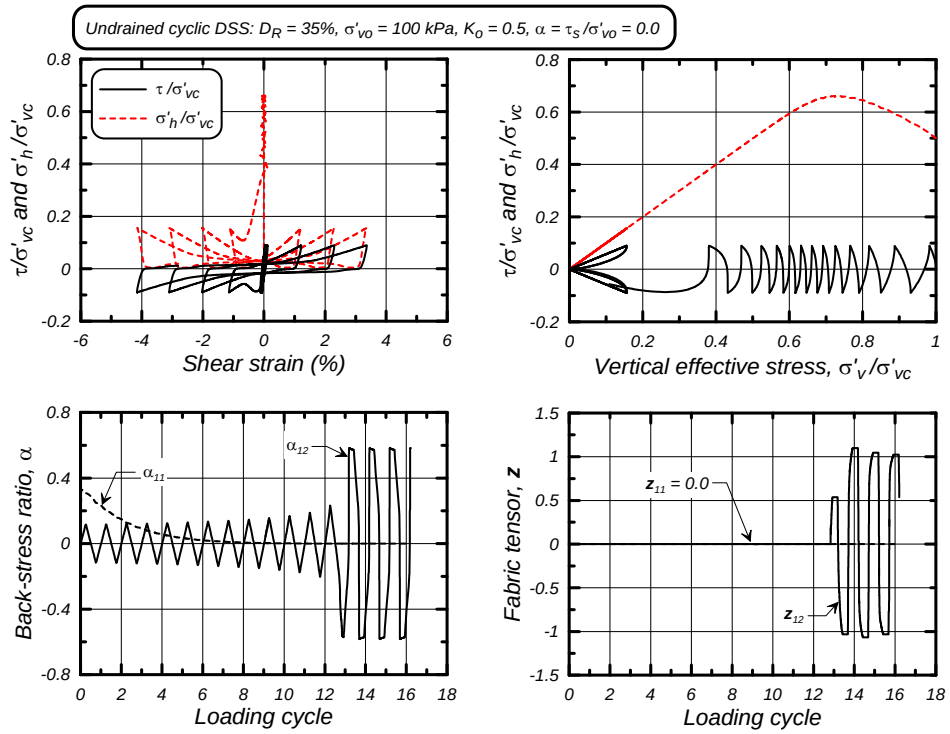

Fig. 4. Undrained cyclic DSS loading response for D_R = 35% with an initial static shear stress ratio of 0.0, showing the variation in stresses, strains, back-stress ratios, and fabric tensor terms.

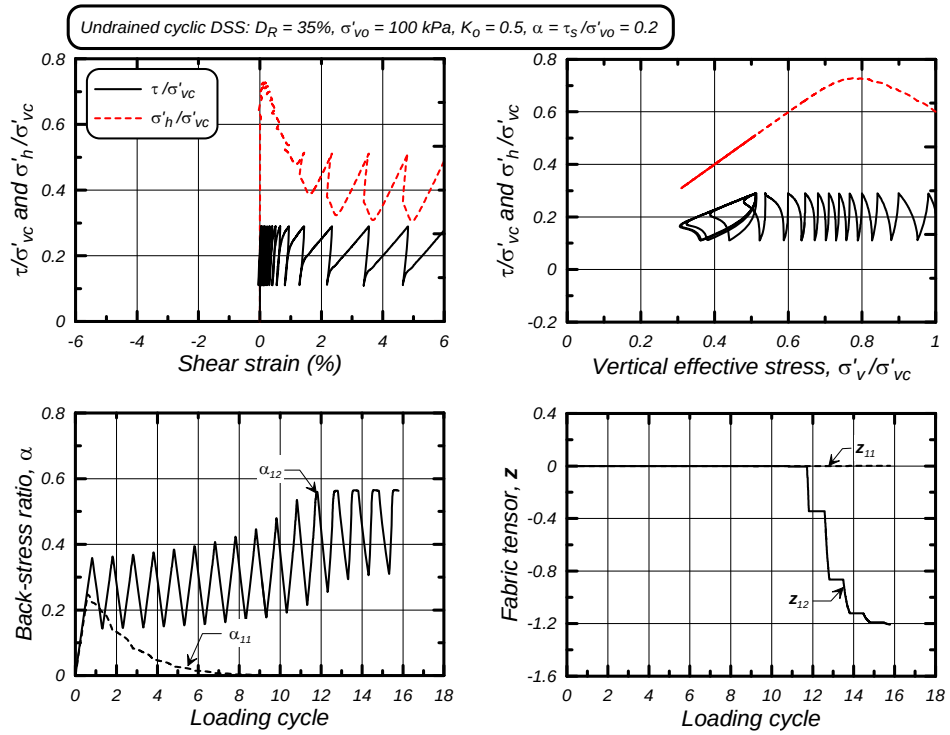

Fig. 5. Undrained cyclic DSS loading response for D_R = 35% with an initial static shear stress ratio of 0.2, showing the variation in stresses, strains, back-stress ratios, and fabric tensor terms.

monotonic and cyclic loading under a range of initial confining stresses and initial static (sustained) shear stress ratios. Some examples of those responses are presented herein.

The response of D_R=35% sand to undrained cyclic direct simple shear (DSS) loading is illustrated in Figs. 4 and 5 for cases having initial horizontal static shear stress ratios (α) of 0.0 and 0.2, respectively. These figures show the stress-strain

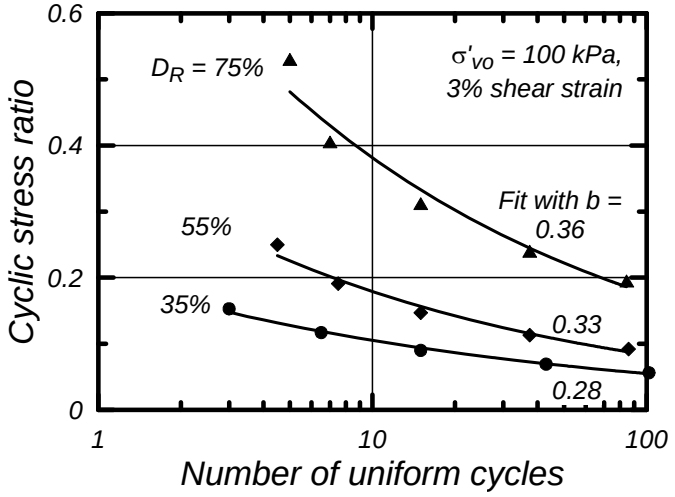

Fig. 6. Cyclic stress ratios versus number of uniform loading cycles in undrained DSS loading to cause single-amplitude shear strains of 3% for D_R = 35, 55, and 75% with a vertical effective consolidation stress of 1 atm. Each set of CSR-N simulations was fit with a power relationship and the exponent b labeled beside each curve

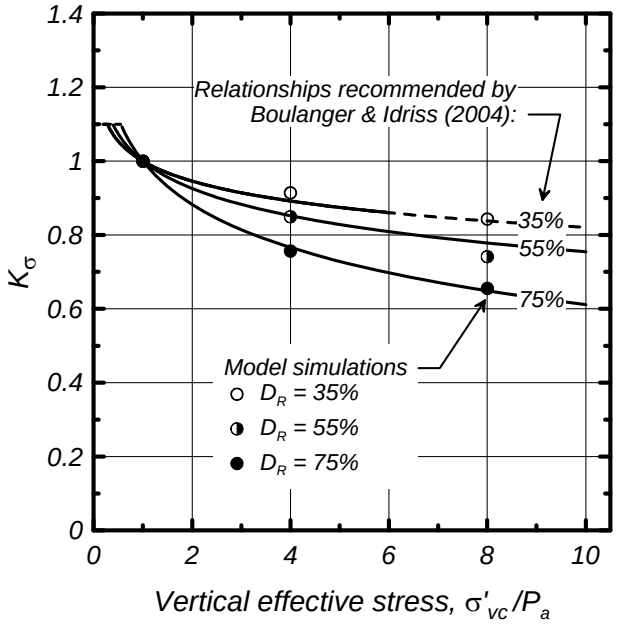

Fig. 7. Comparison of K_σ factors from simulations versus relationships by Boulanger and Idriss (2004).

response, the stress-path response, and time histories for the back-stress ratio and fabric tensor terms. The stress-strain responses for α = 0.0 illustrate the model's ability to progressively reach larger and larger shear strains with continued cyclic loading, rather than locking up in a repeating loop as many plasticity models do. The progressive increases in peak shear strain after the soil has reached a peak excess pore pressure ratio (r_u) greater than 0.98 are realistic in magnitude. The stress-strain responses with α = 0.2 show a progressively accumulation of shear strains in the direction of the initial static shear stress, with the rate and nature of the stress-strain response also being reasonable. The horizontal shear stress does not go through reversal (i.e., change signs) with α = 0.2, and consequently the back-stress ratio and fabric tensor terms also do not go through reversals.

The cyclic stress ratio (CSR) that causes a single-amplitude shear strain of 3% in undrained DSS loading is plotted versus number of uniform loading cycles in Fig. 6 for sand at D_R = 35, 55, and 75%. These results are for a vertical consolidation stress of 1 atm, an initial K_o of 0.5, and zero initial static shear stress ratio. The simulation results in this figure were fitted with a power law, for which the exponent "b" is labeled beside each curve. The slopes of these curves relating CRR to number of loading cycles are in good agreement with typical values obtained in laboratory testing studies (e.g., see Liu et al. 2001 and Idriss and Boulanger 2008).

The effect of overburden stress on CRR is illustrated in Fig. 7 showing the equivalent K_σ values from these simulations, where K_σ is the ratio of CRR to the value of CRR that is obtained when the vertical consolidation stress is 1.0 atm. These K_σ values, determined at 15 uniform loading cycles, are compared in Fig. 7 to the relationships recommended by Boulanger and Idriss (2008). The simulated effects of confining stress are in good agreement with the design relationship by Boulanger and Idriss (2008), as expected because the expression for h_p was calibrated to this relationship.

Drained strain-controlled cyclic loading in DSS for sand at D_R of 35% under vertical consolidation stresses of 1, 4, and 16 atm with K_o=1.0 is shown in Fig. 8, with results also shown for the equivalent modulus reduction (G/G_{max}) and equivalent damping ratio versus cyclic shear strain amplitude. Also shown is the modulus reduction and equivalent damping ratio curves recommended for sands at different depths by EPRI (1993). The simulated modulus reduction and equivalent damping ratio curves depend on the effective confining stress in a pattern and magnitude that is consistent with empirical design correlations, such as the ones by EPRI (1993). The simulated modulus reduction and damping curves are in reasonable agreement with the empirical curves over a fairly broad range of shear strain amplitudes. As shown in Fig. 8, the model's response avoids the problem common to many plasticity models of producing excessively high equivalent damping ratios as shear strain amplitudes exceed about one percent.

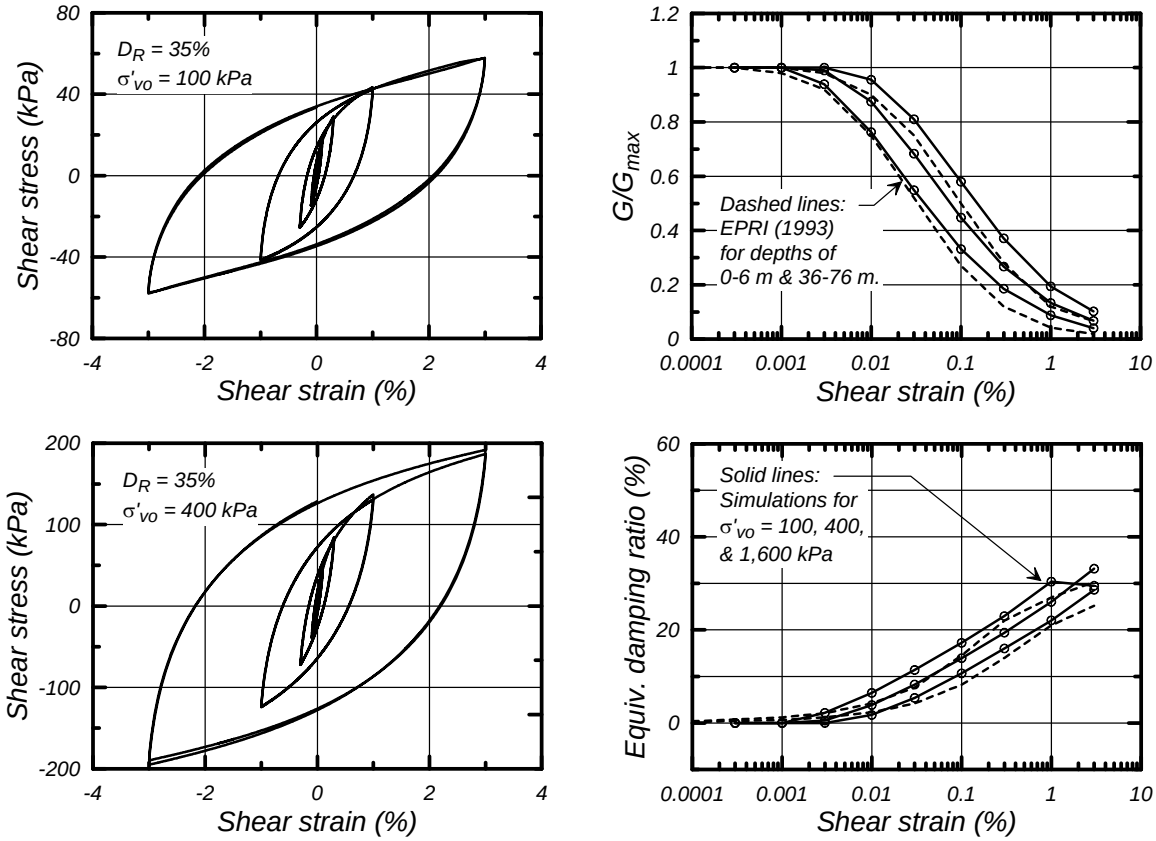

Fig. 8. Drained strain-controlled cyclic DSS loading responses for D_R = 35% under vertical effective consolidation stresses of 1, 4, and 16 atm.

CONCLUDING REMARKS

The sand plasticity model presented herein is built upon the basic framework of the stress-ratio controlled, critical state compatible, bounding surface plasticity model for sand presented by Dafalias and Manzari (2004). Modifications and additions to the model were incorporated to improve its ability to approximate the stress-strain responses important to geotechnical earthquake engineering practice; in essence, the model was calibrated at the equation level to provide for better approximation of the trends observed in empirical correlations commonly used in practice in the U.S. Default values were provided for all but three primary input parameters: G_o which should be calibrated to the estimated or measured in-situ shear wave velocity, h_{po} which is used to calibrate to the estimated in-situ cyclic resistance ratio, and D_R which affects the peak drained and undrained strengths and the rate of strain accumulation during cyclic loading.

The model's behavior was illustrated by example simulations of element loading tests. The model provides reasonable approximations of desired element behaviors and is relatively easy to calibrate. It is currently being evaluated in analyses of data from centrifuge model tests and field case histories.

ACKNOWLEDGMENTS

The author is indebted to Professors Bruce Kutter and Yannis Dafalias for their discussions, insights, and suggestions regarding the formulation, implementation, and description of constitutive models. The assistance of Ronnie Kamai, Katerina Ziotopoulou, and Richie Armstrong in running numerical analyses to evaluate algorithm performance is also greatly appreciated.

REFERENCES

Andrus, R.D., and Stokoe, K.H. (2000). "Liquefaction resistance of soils from shear-wave velocity." J. Geotechnical and Geoenvironmental Eng., ASCE 126(11), 1015–025.

Been, K., and Jefferies, M. G. (1985). "A state parameter for sands." Geotechnique 35(2), 99–112.

Bolton, M. D. (1986). "The strength and dilatancy of sands." Geotechnique 36(1), 65–78.

Boulanger, R. W. (2010). "A sand plasticity model for earthquake engineering applications." Report No. UCD/CGM-10-01, Center for Geotechnical Modeling, Department of Civil and Environmental Engineering, University of California, Davis, California.

Boulanger, R. W., and Idriss, I. M. (2004). "State normalization of penetration resistances and the effect of overburden stress on liquefaction resistance." Proc., 11th Intl. Conf. on Soil Dynamics and Earthquake Engineering, and 3rd Intl. Conf. on Earthquake Geotechnical Engineering, Doolin et al., eds, Stallion Press, Vol. 2, pp. 484-491.

Boulanger, R. W., (2003). "Relating K_α to relative state parameter index." J. Geotechnical and Geoenvironmental Eng., ASCE 129(8), 770–73.

Cubrinovski, M., and Ishihara, K. (1999) "Empirical Correlation between SPT N-Value and Relative Density for Sandy Soils," Soils and Foundations, Japanese Geotechnical Society, Vol. 39, No. 5, pp 61-71.

Dafalias, Y. F., and Manzari, M. T. (2004). "Simple plasticity sand model accounting for fabric change effects." Journal of Engineering Mechanics, ASCE, 130(6), 622-634.

Electric Power Research Institute (1993). Guidelines for site specific ground motions, Rept. TR-102293, 1-5, Palo Alto, California.

Idriss, I. M., and Boulanger, R. W. (2008). *Soil liquefaction during earthquakes.* Monograph MNO-12, Earthquake Engineering Research Institute, Oakland, CA, 261 pp.

Itasca (2009). FLAC – Fast Lagrangian Analysis of Continua, Version 6.0, Itasca Consulting Group, Inc., Minneapolis, Minnesota.

Konrad, J.-M. (1988). "Interpretation of flat plate dilatometer tests in sands in terms of the state parameter." Geotechnique 38(2), 263–77.

Liu, A. H., Stewart, J. P., Abrahamson, N. A., and Moriwaki, Y. (2001). "Equivalent number of uniform stress cycles for soil liquefaction analysis." J. Geotechnical and Geoenvironmental Engineering, ASCE 127(12), 1017-1026.

Manzari, M. T., and Dafalias, Y. F. (1997). "A critical state two-surface plasticity model for sand." Geotechnique, 47(2), 255-272.

Salgado, R., Boulanger, R. W. and Mitchell, J. K. (1997). "Lateral Stress Effects on CPT Liquefaction Resistance Correlations." Journal of Geotechnical and Geoenvironmental Engineering, ASCE, Vol. 123, No. 8, August, pp 726 – 735.